- D2.1 – Report on present state-of-art for sensors Li-ion batteries -

- VERSION -

VERSION	*DATE*
1	8/12/20

- PROJECT INFORMATION -

GRANT AGREEMENT NUMBER	955930
PROJECT FULL TITLE	INNOVATIVE PHYSICAL/VIRTUAL SENSOR PLATFORM FOR BATTERY CELL
PROJECT ACRONYM	INSTABAT
START DATE OF THE PROJECT	01/09/2020
DURATION	3 years
CALL TOPIC	H2020-LC-BAT-13-2020
PROJECT WEBSITE	www.instabat.eu

- DELIVERABLE INFORMATION -

WP NO.	2
WP LEADER	UAVR
CONTRIBUTING PARTNERS	CEA; CNRS; INFINEON
NATURE	REPORT
AUTHORS	M. Nascimento, C. Marques, and J. Pinto
CONTRIBUTORS	C. Gervillié, L. Blanquer, S. Genies, Y. Reynier, L. Beaurenaut, A. Zoepfl, T. Roessler, O. Raccurt, and J-M. Tarascon
CONTRACTUAL DEADLINE	20/12/20
DELIVERY DATE TO EC	15/12/20
DISSEMINATION LEVEL (PU/CO)	PU

- ACKNOWLEDGMENT -

This project has received funding from the European Union's Horizon 2020 research and innovation program under grant agreement No 955930.

- ABSTRACT/SHORT SUMMARY –

Nowadays, battery management systems (BMS) measure only externally accessible parameters such as voltage, current and temperature to ensure safe operation. However, other (internally accessible) parameters could also be monitored, allowing a better control of the battery by the BMS and thus an increased quality, reliability, life (QRL) and safety of the battery. Today, the lack of knowledge about the state of each individual battery cell makes it necessary to overdesign the battery to ensure reliable operation. More information is desirable for real-time internal cell state monitoring, e.g. to calculate accurate cell indicators (such as States of Charge (SoC), Health (SoH), Power and Energy) and early indicators for cell failure (State of Safety). The increase in accuracy of these indicators would allow the BMS to better control the battery cells.

Although progress towards instrumental miniaturization, as well as non-disturbance and compatibility with cell internal environment, has been achieved over the years, we are still far from comprehensively monitoring batteries in "real life." An interesting compromise could also arise from the use of a reduced set of measurements (provided by a few physical sensors), associated with virtual sensors to estimate other internal variables. In particular, electrochemical and thermal virtual sensors could fill in the information gaps resulting from the restrictions on direct measurements.

Finally, the lack of knowledge about cell use patterns and degradation during the life of the battery currently limits the feasibility of cells second life and recyclability. New non-invasive integrated sensors based on optical fiber, photo-acoustic and reference electrode technologies will be improved/developed and will allow to know in real time the evolution of internal battery key parameters. This deliverable gives a detailed state-of-the-art of each proposed physical sensor that will be developed on INSTABAT project.

- TABLE OF CONTENTS -

Contents

1. Current state-of-the art and limitations

The scarcity of information regarding the interior of the cell currently hinders improvement of the accuracy and predicting capabilities of current BMS models, while equally limiting attempts to refine the battery thermal design due to the absence of heat-transfer information. This has led to increasing interest for imaging in time and space the thermal flows within a cell using temperature sensors. In addition, monitoring the temperature and thermal flows of Lithium-Ion Battery (LIB) cells is fundamental to ensure that they operate in safe conditions[1]. Typically, temperature changes are monitored, outside the cell, by electronic sensing devices, such as thermocouples, thermally sensitive resistors (thermistors or resistance thermometers), infrared thermography and pyrometers[2]. However, in addition to (1) low resolution and accuracy (infrared thermography, thermocouples (±1.5°C; ±25%)), (2) bulky measurement setup e.g. complex wiring (thermocouples), or (3) high volume/size preventing them from being inserted in a battery cell (thermistors), some of these sensors are not suitable to be embedded in battery cells due to the electrochemical harsh environment. Alternative solutions, with higher precision, multipoint capabilities, immunity to electromagnetic interference, chemical inertness, non-conductivity and small size/low invasiveness, are sensors based on OFs. Moreover, OFs are highly flexible and can be multiplexed. Depending on the application, these sensors can be tailored regarding their dimensions and sensitivity[3]. In the last years, OF sensors were implemented on LIBs (cylindrical, prismatic and pouch cell configurations) to monitor internal and external temperature distributions[4] or chemical reaction such as lithiation of graphite electrodes[5], state of charge[6] or electrolyte degradation and SEI composition[7].

Furthermore, batteries are breathing objects that expand and contract upon cycling, with volume changes that can reach up to 10 %. These changes, together with the electrode volume expansion associated to the SEI growth, lead to important mechanical stress inside the battery materials (like cracks) that are detrimental to battery performances. Methods, to sense intercalation strain and cell pressure, are equally critical for controlling the solid-electrolyte interphase (SEI) dynamics that affects the SoC as well as SoH of batteries. This explains the already existing studies aiming to know the influence of such parameters on the cell performances. Methods used so far to measure pressure and strain are not entirely satisfactory: strain-gauges fall short of providing spatial information and cannot internally sense battery cells (due to their electrochemical environment). Acoustic Emission technique requires copious wiring to connect the acoustic transducers used for signal emission and reception. However, wireless devices could be developed to circumvent this issue[8]. Methods based on optical fibers have recently opened new opportunities[9].

[1] (a) P. K. Leung, et al., J. Power Sources (2014) 271. (b) P. Wang, et al., Extreme Mech. Lett. (2016) 9. (c) W. Xianming, et al., J. Electrochem. Soc. (2007) 154. (d) H. L. Jae, et al., J. Power Sources (2003) 119-121. (e) D. Yih-Shing, et al., J. Therm. Anal. Calorim (2018). (f) T. M. Bandhauer, et al., J. Electrochem. Soc. (2011) 158. (g) Q. Wang, et al., J. Power Sources (2012) 208.

[2] (a) M. S. K. Mutyala, et al., J. Power Sources (2014) 260. (b) Y. Fu, et al., J. Power Sources (2015) 273. (c) L. H. J. Raijmakers, et al., Applied Energy (2019) 240. (d) Z. Li, et al., J. Power Sources (2013) 241. (e) M. Yildiz, et al., Int. Com. Heat Mass Transfer 75 (2016) 311-314. (f) P. Wang, et al., Extreme Mech. Lett. (2016) 9. (g) Z.J. Wang et al., Proceedings of SPIE (2011) 8193. (h) J. B. Robinson, et al., ECS Electrochemistry Lett. (2015) 4(9). (i) U. S. Kim, et al., J. Power Sources (2008) 180. (j) S. Panchal, et al., Int. Commun. Heat Mass Transf. (2016) 71

[3] K. T. V. Grattan, et al., Optical fiber sensor technology: Applications and Systems. Kluwer Academic Publishers, London, (1999) 3 357-363.

[4] (a) M. Nascimento, et al., Measurement (2017) 111. (b) S. Novais, et al., Sensors (2016) 16, 1394. (c) G. Yang, et al., Measurement (2013) 46 3166-3172. (d) M. Nascimento, et al., Appl. Therm. Engineering (2019) 149. (e) M. Nascimento, et al., Batteries (2018) 4, 67. (f) M. Nascimento, et al., Batteries (2018) 4 23. (g) M. Nascimento, et al., J. Power Sources (2019) 410-411.

[5] (a) Ghannoum, A.; et al. (2016), , ACS Applied Materials and Interfaces 8(29), 18763-18769.
(b) Ghannoum, A.; et al. (2017), Proceedings of IEEE Sensors. (c) Ghannoum, A.; et al. (2017), ACS Applied Materials and Interfaces 9(47), 41284-41290.

[6] Hedman, J.; Nilebo, D.; Larsson Langhammer, E. & Björefors, F. (2020), 'Fibre Optic Sensor for Characterisation of Lithium-Ion Batteries. ChemSusChem, 13(21), pp. 5731-5739.

[7] a) Yamanaka, T.; et al. (2017), Japanese Journal of Applied Physics 56(12), 128002. b)Yamanaka, T.; et al. (2017), Electrochemistry Communications 77, 32 – 35. c) Yamanaka, T.; et al. (2017), Journal of Power Sources 359, 435 - 440.

[8] S. Shaikh, PhD thesis, 2016, https://mountainscholar.org/handle/10976/166948.

[9] Huang, J. et al. Nat Energy 5, 674–683 (2020).

Lithium concentration into the cells and especially in the interfaces is relatively difficult to measure. The local lithium concentration can currently be determined by post-mortem analysis[10] but this technique is destructive and does not allow monitoring the cell in the battery pack. Other methods for in operando measurements were developed like nuclear magnetic resonance[11], neutron scattering[12] or other techniques using large-scale instruments[13]. These methods are, however, not applicable to measure the concentration of Li-ion inside the battery as they are not implementable in the electrochemical environment of a battery cell.

Another indication of safety-critical processes in a LIB cell is the formation of critical gases, such as HF and CO_2. In the past, pressure sensors have been used to obtain at least basic information related to this effect during battery operation. However, to some extent, gas formation (and the associated pressure increase in the cell) is part of the normal cell processes during charging and discharging[14]. For a more detailed evaluation of the SoX of the cell, it would therefore be advantageous to obtain further information about the presence of individual gases and their concentrations, and not just the pressure inside the cell.

CO_2 is one of the gases expected to develop in rather large amounts at the onset of safety-critical processes in LIB cell. Therefore, a technology to measure continuously the CO_2 content in the battery gaseous atmosphere, without disturbing the cell electrochemistry, could provide an early warning for such processes. To our knowledge, up to now the connection of a CO_2 detector to LIB cell for this purpose has not yet been realized.

Fundamental electrochemical studies, regarding LIB cells, require the implementation of a reference electrode inside the cell to be able to record the potential profile and characterize the kinetics properties and the interface structure of each electrode individually[15]. Obtaining such data proves to be essential to better understand the electrochemical processes and the aging mechanisms that are generated by cycling, in particular at different temperatures, with the perspective to limit damaging phenomena, considering lithium plating. In addition to these physical measures, "absolute" potential, impedance and polarization could also be attained.

2. State-of-art of the four proposed physical sensors

2.1 Optical Fiber / Fiber Bragg Grating (OF/FBG)

A fiber Bragg grating (FBG) is a local modulation of the refractive index in the OF which can be created by an appropriate sideways illumination with UV light (spatial fringe pattern) of a photosensitive OF, as shown in **Figure 1**(A)[16]. So, the measured information is usually encoded in a shift of the Bragg wavelength as exhibited in **Figure 1**(B).

[10] T. Waldmann, et al., J. Electroch. Soc. (2016) 163.

[11] (a) Y. J. Lee, et al., J. American Chemical Soc. (1998) 120. (b) S. Surblé, et al., J. Power Sources (2018) 393.

[12] C. von Lüders, et al., J. Power Sources (2017) 342.

[13] (a) P. Harks, et al., J. Power Sources (2015) 288. (b) C. P. Grey and J. M. Tarascon, Nature Materials (2016) 16.

[14] J. Schmittt, et al., Poster at the "Kraftwerk Batterie / Advanced Battery Power 2019", Aachen 2010.

[15] Electroanalytical Methods Guide to Experiments and Applications, Springer; Edition: 2nd ed. 2010 (11 november 2014).

[16] (a) D. C. Johnson, et al., Appl. Phys. Lett. (2008), 32, 647. (b) W. Lutang et al., IntechOpen (2017).

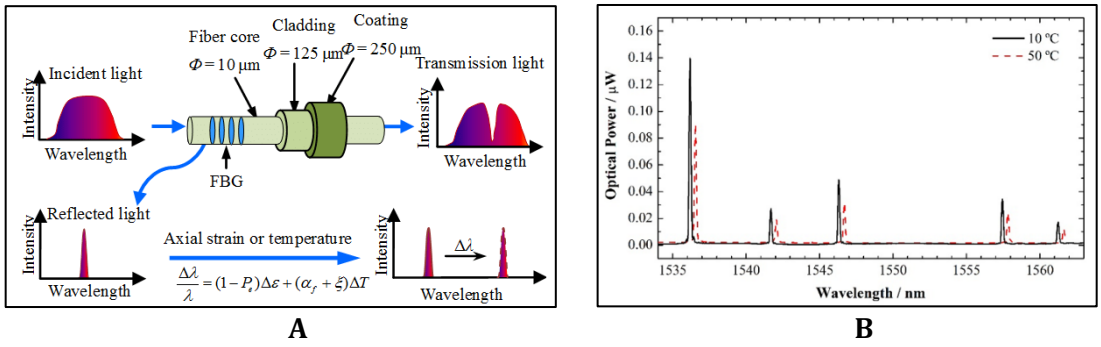

Figure 1. A) Optical fiber with a FBG sensor recorded on the fiber core. The wavelength peak of the FBG sensor changes with strain and temperature shifts, suffering from large cross-sensitivity. B) Spectra of a FBG network at two different temperatures[17].

The reflected spectrum is centered on the Bragg-wavelength (λ_B) and depends on the effective index of refraction (n_{eff}) and on the Bragg period (Λ) of the grating according to the well-known Bragg equation:

$$\boldsymbol{\lambda_B = 2 n_{eff}\, \Lambda_B} \qquad \text{(eq.1)}$$

By inscribing several FBGs with different grating periods in the same optical fiber, an array of gratings can be manufactured. This allows the user to monitor different positions in the structure with only one sensor line. Figure 1 (B) shows the spectrum of five FBGs placed in the same fiber, and the two different spectra at two different temperatures.

FBGs are sensitive to several physical parameters, in particular to strain/pressure and temperature at the same time, which results in considerable cross sensitivity.

In particular, the effective refractive index is modified through the thermo-optic and strain-optic effects, respectively. Hence, from Equation (1), the Bragg wavelength shift $\Delta\lambda_B$ due to strain $\Delta\varepsilon$ and temperature ΔT variations is given by:

$$\boldsymbol{\Delta\lambda_B = 2\left(\Lambda \frac{dn_{eff}}{dT} + n_{eff}\frac{d\Lambda}{dT}\right)\Delta T + 2\left(\Lambda \frac{dn_{eff}}{d\varepsilon} + n_{eff}\frac{d\Lambda}{d\varepsilon}\right)\Delta\varepsilon} \qquad \text{(eq.2)}$$

The first term in Equation (2) represents the effect of temperature on the Bragg wavelength and the Bragg wavelength shift due to thermal expansion comes from the modification of the grating spacing and the refractive index.

Many procedures have been proposed to discriminate simultaneously strain/pressure and temperature. The most straightforward is to use two different FBGs: one FBG is dedicated to strain/pressure measurement and the other one simultaneously detects strain/pressure and temperature. However, this method can be challenging when it is proposed to monitor specific parameters inside electrochemical materials, such as batteries. Certain methods are based on the use of different sensing elements that have different responses to strain/pressure and temperature[18]. All these methods have good response to strain/pressure and temperature; however, they are inappropriate for precise measurements due to low spatial resolution because their dimension is very high (3 cm)[19].

In the recent years, this type of optical fiber sensors were extensively used as a tool addressed at LIB monitoring. UAVR partner has pioneered on the development of optical fiber sensors networks based on FBGs

[17] M.Nascimento. PhD Thesis. 2019

[18] (a) M. R. Mokhtar, et al., IEEE Sens. J. (2012) 12. (b) O. Frazão, et al., Meas. Sci. Technol. (2005) 16. (c) C. Fernández-Valdivielso, et al., Sens. Act A (2002) 101.

[19] L. A. Ferreira, et al., Opt. Eng. (2000) 39.

and their integration in (1) commercially available Li-ion batteries (coin, cylindrical and prismatic) and (2) prefabricated batteries in a laboratory environment (pouch cells). The objective was to monitor in situ, in operando and in real time, the internal and external variations of temperature and strain, under different environmental conditions and different charge and discharge rates. In pouch cells, the discrimination of internal strain and temperature was achieved with hybrid sensors by a cross sensitivity matrixial method[20].

Through comparative studies, it is clearly demonstrated that FBGs offer a better resolution together with a faster response time than thermocouples[21]. Sensing networks based on FBGs were developed to monitor temperature variations both internally and externally in a pouch cell, in two different locations, and were also used to discriminate simultaneously external bidirectional strain and temperature in a prismatic LIB, using an independent strain-free FBG. Moreover, owing to the feasibility to insert numerous (36) FBGs in a network, they were able to realize a temporal and spatial thermal mapping of the interfaces of a lithium battery pack, as shown in **Figure 2**. By analyzing the thermal contours at the beginning/end of charge/discharge, they were able to visualize the presence of a longitudinal gradient concentration and to identify hot spots near the positive tab collectors between two batteries.

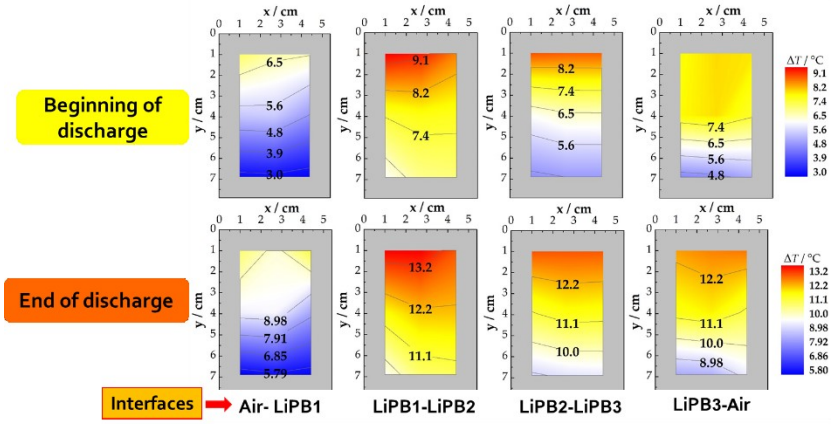

Figure 2. Surface LIB pack thermal mapping performed by a network of 36 FBG sensors, during discharging at 1.4C.

This sensing technology was also recently implemented to determine fast and slow ion diffusion processes in Li-ion pouch cells[22] and to monitor the strain evolution of LIB electrodes[23]. Overall, whatever the cell configuration and the various Li-ion chemistry tested, FBGs are shown to be perfectly suitable for achieving reliable cell temperature imaging provided we find clever ways, compatible with the manufacturing process, to simply integrate them within the cell without jeopardizing cell performance and safety.

UAVR group was a pioneer in the study and simultaneously discriminate of internal strain and temperature shifts in Li-ion pouch cells, based on the development of a hybrid optical sensor that combines the wavelengths of an FBG sensor and a Fabry-Perot interferometer, as shown in **Figure 3** (A). Galvanostatic cycling at different C-rates was applied to the cell and the evolution of strain and temperature were followed with the proposed sensor[24].

[20] (a) M. Nascimento, et al., J. Power Sources (2019) 410-411. (b) M. Nascimento, et al., Appl. Therm. Engineering (2019) 149. (c) M. Nascimento, et al. (2018) Batteries 4(4), 67. (d) M. Nascimento, et al., Batteries (2018) 4(2), 23. (e) M. Nascimento, et al., Measurement (2017) 111. (f) S. Novais, et al., Sensors (2016) 16. (g) G. Yang, et al., Measurement (2013) 46.

[21] M.J. Ross, et al., P. Sensors (2019) 19, 1432.

[22] L.W. Sommer, et al., J. Power Sources (2015) 296.

[23] C -J. Bae, et al., Energy Technol. (2016) 4.

[24] M. Nascimento, et al., J. Power Sources (2019) 410-411.

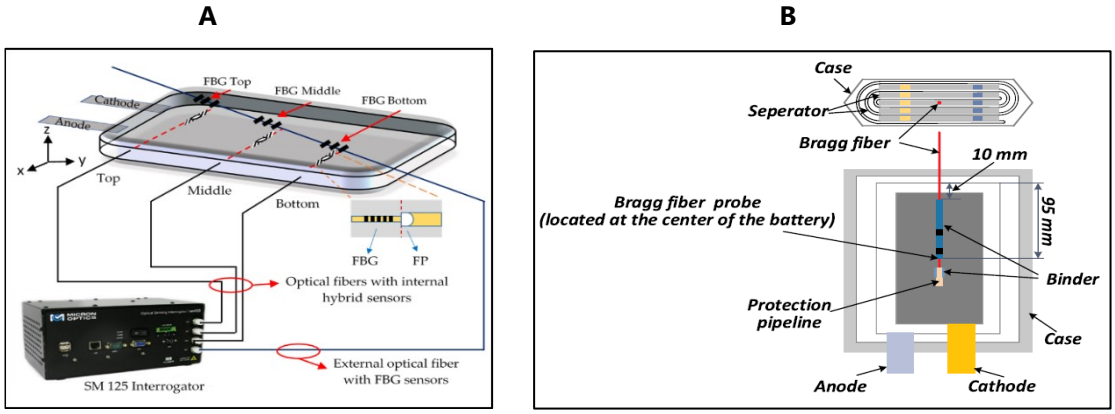

Figure 3. Experimental setup diagram of the external (A) and internal (B) optical sensors network used to temperature and strain monitoring of the Li-ion pouch cell[25].

Another group demonstrates that integrated FBGs in batteries are an interesting option for early detection of electrode strain and temperature overall operational and safety-critical scenarios of the Li-ion cell[26]. This group reports the feasibility to prepare high-performance large-format Li-ion pouch cells for EV applications with integrated FBGs attached to the electrode[27]. Similarly, Raghavan et al.[28], as can be seen in **Figure 3** (B), implemented an internal state monitoring apparatus based on the embedded FBG optical sensor, whose refractive index and refracted wavelengths are both subject to change with the battery's internal strain and temperature. Therefore, by measuring the change of the refracted wavelength, the strain and temperature inside a Li-ion battery can be estimated. The embedding position and the FBG optical sensor coated with corrosion-resistant material are essential to the success of this internal state monitoring apparatus.

They further demonstrate the seal integrity, capacity retention and projected lifecycle. All of them are comparable to contemporary EV cells without integrated sensors. No major adverse effects on the cell life from integrated fiber could be observed after at least 1000 cycles. Based on the achieved strain accuracy they show that the strain measured using FBG sensors can be used to estimate SoC with less than 2.5 % error under different temperature conditions and under dynamic cycling. However, an inherent drawback of this sensing technology is that it suffers from a large cross sensitivity to temperature, pressure and/or strain shifts. Simultaneous discrimination can be obtained by recording FBGs in polarization maintaining fibers: FBGs written in high-birefringent (Hi-Bi) OFs are able to simultaneously discriminate temperature and strain[29] (longitudinal and transverse components). The basis for measuring two parameters with an FBG is to have a different sensitivity of the Bragg wavelength. This is achieved in Hi-Bi gratings because the shift of the reflection bands, for each polarization, is different and depends on the angle of the application of the external load. The displacement of both Bragg wavelengths can be used in a matrix equation to determine the two physical parameters: temperature and strain. To sense in one single point in space, both FBGs are written in the same position of the Hi-Bi fiber. As a consequence of the internal stress profile, the optical reflection spectrum of a FBG written in Hi-Bi fibers, with non-polarized light focused on the fiber, has a two-peak structure corresponding to the two orthogonal polarization modes of the fiber (see **Figure 4** (A); the X and Y polarizations of the LP01 modes are split and each one has a different effective index. These linear polarizations are the slow (X-axis) and fast (Y-axis) modes associated with the principal directions of the refractive index

[25] (a)M. Nascimento, et al., J. Power Sources (2019) 410-411; (b) Z. Liao, et al., J. Power Sources (2019) 436.

[26] L.W. Sommer, et al., J. Power Sources (2015) 296.

[27] C.-J. Bae, et al., Energy Technology (2016) 4.

[28] (a) A. Raghavan, et al., J. Power Sources, 341 (2017), 466-473. (b) A. Ganguli, et al., J. Power Sources, 341 (2017), 474–482. (c) A. Fortier, et al., Energies 10 (838) (2017) 1–11.

[29] I. Abe, et al., Meas. Sci. Technol. (2004) 15.

profile of the fiber. To use an OF sensor composed of FBG in Hi-Bi fiber it is necessary to characterize the grating properties in the presence of the parameters to be measured, as the specific dependence of these properties can induce different responses of the sensor system[30].

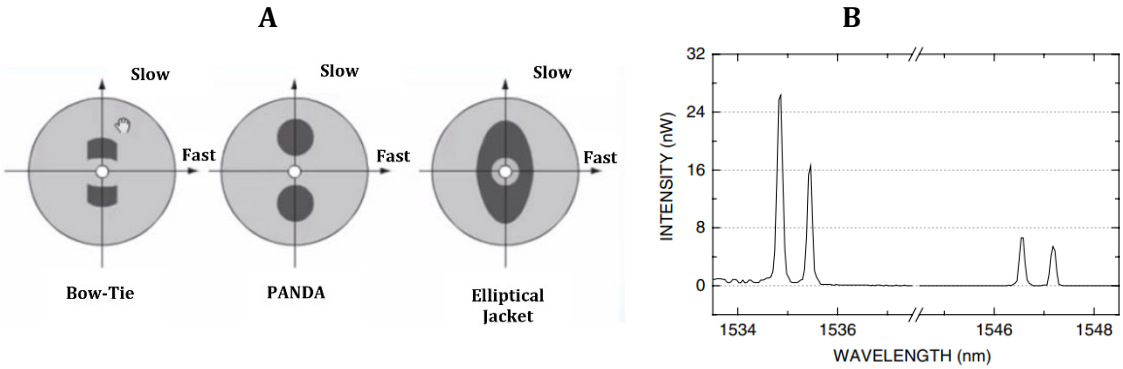

Figure 4. A) Cross-sections of Bow Tie, Internal Elliptical Cladding, and Panda geometries. B) Optical reflection spectrum from the structure with two superimposed Bragg gratings in Internal Elliptical Cladding Hi-Bi fiber. FBGs were inscribed using different phase masks.

Another fiber sensing technology that is becoming increasingly popular are microstructured optical fibers (MOFs) in which can be inscribed FBGs. More specifically, the design flexibility of such MOFs allows developing FBG optical sensors that exhibit selective sensitivities, e.g. to pressure, axial and transverse strain or shear stress, whilst being negligibly cross-sensitive to temperature changes[31]. Since the birefringence of that MOF is not sensitive to temperature changes, the strain and/or pressure measurement is independent of temperature variations. MOF technology allows achieving optical sensors with sensing characteristics that cannot be obtained with conventional fiber technology. MOF sensing approaches and techniques have been reviewed for example by Frazão et al.[32], Canning[33] and Pinto et al.[34]. This sensing technology was also recently used by some researchers from CNRS partner, by showing that collected optical sensing signals are rich with chemical information that is particularly insightful to understanding parasitic reactions and interfacial growth dynamics, as can be seen on **Figure 4** (B). Additionally, they demonstrate the benefit of combining signals from different optical fibers (SMF and MOF) for performing heat-flow measurements, which also allow for probing of cells heat capacity contributions[35] (see **Figure 5**).

[30] I. Abe, et al., Meas. Sci. Technol. (2004) 15.

[31] F. Berghmans, et al., Proceedings of EWSHM (2014) hal-01021256.

[32] O. Frazao, et al., Laser & Photonics Reviews (2008) 2(6).

[33] J. Canning, J. of Sensors (2012) 598178.

[34] A.M.R. Pinto, et al., J. of Sensors (2009) 871580.

[35] Huang, J. et al. Nat Energy 5, 674–683 (2020).

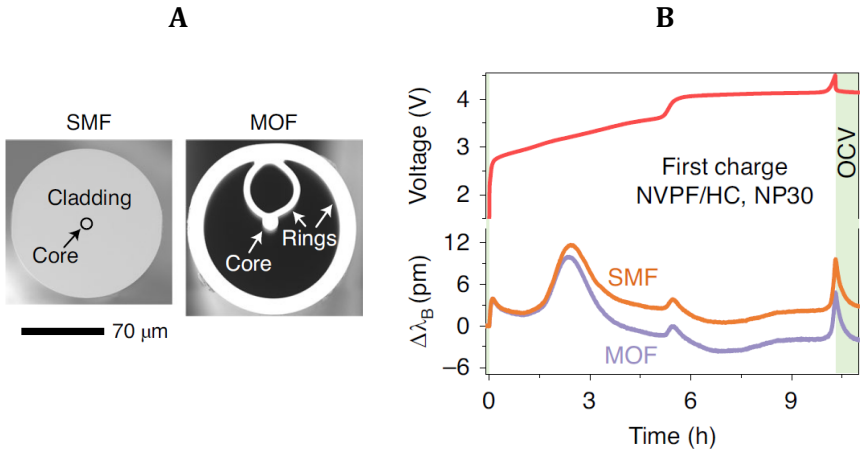

Figure 5. Probing temperature and pressure dynamics inside batteries and its implications on the SEI. A) The cross-section SEM images of SMF and MOF. The MOF is very sensitive to hydraulic pressure due to its very high air-filling fraction. B) The measurements of time-resolved voltage (red) and ΔλB of SMF-FBG (orange) and MOF-FBG (purple) during the first charge of a single NVPF/HC cell at C/10.

2.2 Optical Fiber / Thermoluminescence (OF/LumT) and Optical Fiber / Luminescence (OF/LumL)

Another option to use OF sensors as a thermometer is luminescence thermometry, which has been developed for 20 years[36] to measure temperature in many domains where other techniques were not applicable. However, this method has never been applied in the field of batteries. The method relies on the temperature dependence of the optical properties of specific luminescent materials. As **Figure 6** suggests, different types of detection techniques (e.g. peak energy and intensity, excited lifetime and rise time) can be used depending on the material properties. The most sensitive technique for thermoluminescence used the ratiometry.

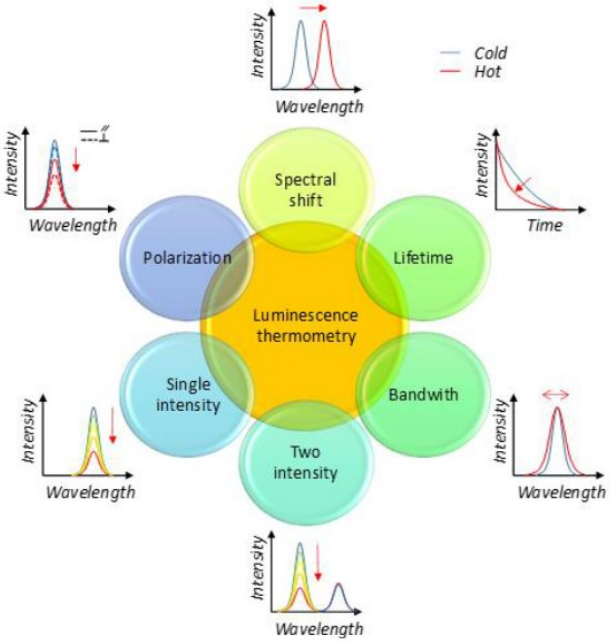

Figure 6. Modification of luminescence due to increase of temperature.

[36] (a) M. McSherry, et al., Sensor Review (2005) 25. (b) J. Xiong et al., Scientific Reports (2017) 7. (c) X. Wang, et al., Chem. Soc. Rev. (2013) 42. (d) C. D. S. Brites, et al., Advanced Optical Materials (2018) 6.

In this case, monitoring of the intensity of two radiative transitions is used (at two different wavelengths). The ratio between the two intensity or area under the peak varied with temperature. An example of this type of thermoluminescent material is given in **Figure 7** (from reference 39). In this case the peak at 540 nm is the reference and the peak at 525 nm rises with temperature.

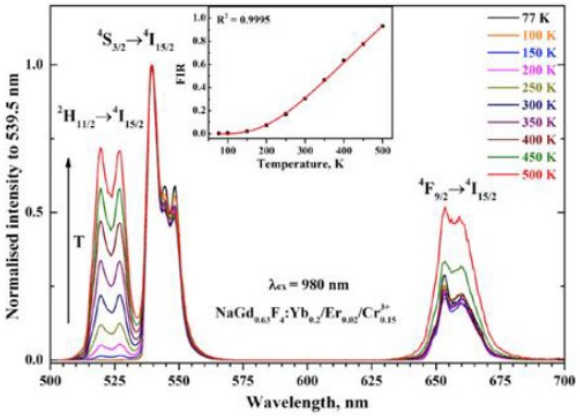

Figure 7. Thermoluminescence variation of $NaGdF_4$:Yb/Er/Cr between 77K and 500K [39].

Luminescence thermometry combines a high relative thermal sensitivity (>1% K^{-1}) with a good spatial resolution (depending of the size of probe <10 µm) and short response times (<1 ms). This technique is widely used in environmental science, where it is difficult to use other standard methods due to aggressive environments, biological or confined[37]. A large variety of materials can be used as thermoluminophore (inorganic, organic or hybrid). From the different ways to monitor the temperature by luminescence, the ratiometry is probably the best way (difference between two peaks, one as reference and another with temperature dependent intensity)[38]. The variation of luminescence can cover a large scale of temperature. One example has been done by C. D. S. Brites et al. between 77 to 500 K[39] and a more recent publication from M. Łukaszewicz et al.[40] from 175 K to 895 K.

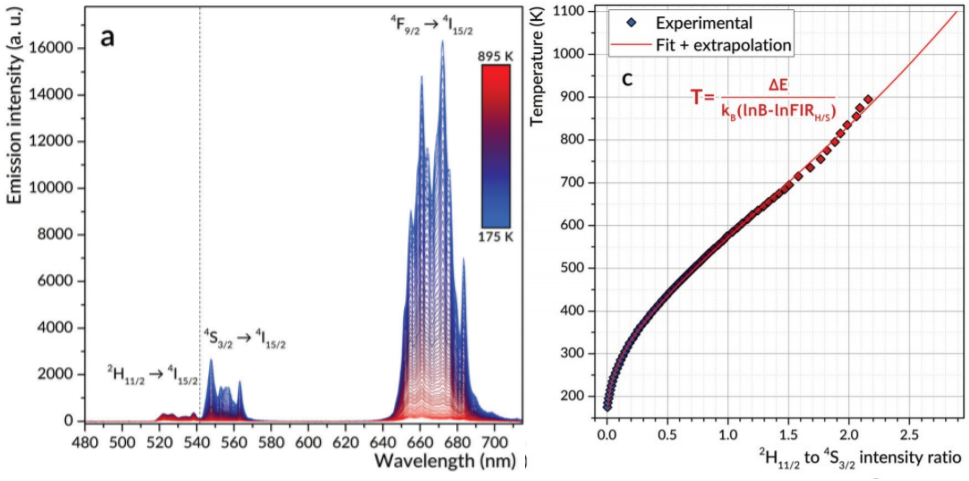

Figure 8. Thermoluminescence variation of $Y_2O^{3-}Er^{3+}$, Yb^{3+} ceramic between 175 to 895 K.

[37] X. Wang, et al., Chem. Soc. Rev. (2013) 42.

[38] C. D. S. Brites, et al., Advanced Optical Materials (2019) 7.

[39] C. D. S. Brites, et al., Advanced Optical Materials (2018) 6.

[40] M. Łukaszewicz et al, J. Mater. Chem. C, 2020, 8, 1072--1082

The scale of interest for battery is between -40 °C to 150 °C. Up to this temperature, thermal runaway of battery is uncontrollable.

Other important criteria for thermoluminescent material regarding the application is the excitation wavelength and the stockes or antistockes shift. Excitation wavelength must not be absorbed or affect the near environment of the probe. That's an arch UV source shouldn't be used as excitation source for thermoluminescent materials. UV light can degrade materials and especially polymers as separators. The table below gives some example of thermoluminescent materials with excitation, emission wavelengths, sensitivity and the scale. Of course, sensitivity is one of the major requirements for a good thermal probe. **Table 1** shows the list of inorganic thermoluminophores doped by lanthanides. This table was compiled by C.D.S. Brites et al.[38]. In this study, many thermoluminophore were studied in the range of low temperature and around the ambient temperature. Few of them were studying in the range of interest for battery. This limitation of temperature range is often due to the domain where this material was applied (biotechnology, materials science, etc...). And it's not a synonym that these materials don't be adapted for the range of interest in our cases.

This luminescent material can be easily deposited onto an optical fiber, as presented in **Figure 9**. In the state-of-the-art, many examples of luminescent materials such as particle and molecule are already published especially for biological applications[41].

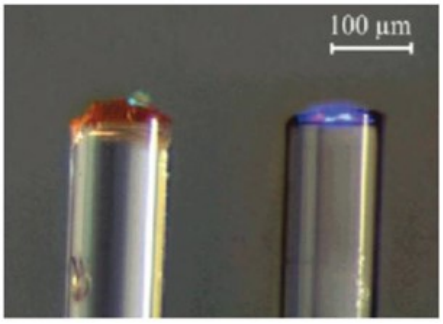

Figure 9. Optical fiber with luminescent probe for in vivo measurement of temperature by luminescence.

It is necessary to develop small detectors able to measure in operando the Li-ion concentration in the cells without perturbing the cell performance and safety. Detecting and monitoring the concentration of metallic ions (such as lithium) in liquid medium and in complex environment was extensively studied for more than 30 years in other fields (e.g. environmental and clinical research[42]). From the four different techniques that were already developed for measuring Li-ion in liquid environment, two of them are compatible to be used as small sensors for battery cell in situ measurement. The first technique is based on using conductive polymers placed on a surface with metallic contact. The adsorption of ions on the surface of probe materials induces a modification of the resistance. However, this type of sensor is difficult to miniaturize and requires electrical measurement[43]. The second method is based on the use of chromophore as a probe with ion sensitivity.

[41] (a) X. Wang, et al., Chem. Soc. Rev. (2013) 42. (b) P. Golden, et al., IEEE Transactions on Biomedical Engineering (1994) 41. (c) G. P. Anderson, et al., IEEE Transactions on Biomedical Engineering (1994) 41. (d) Y. Huang et al, Inorg. Chem. 2020, 59, 19, 14229–14235

[42] M. Kamenica, et al., Sensors (Switzerland) (2017) 17.

[43] T. Gunnlaugsson, et al., Tetrahedron (2004) 60.

Table 1. *List of Lanthanides doped inorganic thermoluminophore from Brites et al[38] with range of temperature, sensitivity and optical parameters.*

Δλ	Material		ΔT [K]	S_m [% K^{-1}]	T_m [K]	δT [K]	Optical parameter	Ref.
VIS	Ln-HL (Ln = Eu, Tb)	MOFs	4–290	31	4	–	Two intensities	[186]
	$Sr_2GeO_4:Pr^{3+}$	NPs	17–600	7.5	22	0.1	Two intensities	[197]
	$Eu(keto)_3(H_2O)$	C	12–300	7.0×10^{-2}	50	–	Bandwidth	[169]
				1.0		–	Spectral shift	[169]
	$Y_2O_3:Eu^{3+}$	NPs	10–670	7.8×10^{-2}	70	–	Bandwidth	[165]
	$NaGdF_4:Pr^{3+}/Er^{3+}$ @$NaYF_4:Yb^{3+}$	CS	83–323	9.5	83	–	Two intensities	[194]
	$Y_2O_3:Yb^{3+}/Ho^{3+}$	UCNPs	10–300	1.6	85	–	Two intensities	[201]
	$TiO_2:Tm^{3+}$	NPs	85–750	3.0×10^{-4}	85	–	Bandwidth	[168]
	$NaYbF_4:Tm^{3+}$@SiO_2	UCNPs	100–700	5.6×10^{-2}	100	–	Bandwidth	[166]
	$NaYF_4:Pr^{3+}$	P	120–300	4.7	120	–	Two intensities	[239]
	$(Me_2NH_2)_3[Eu_3(FDC)_4(NO_3)_4]\cdot4H_2O$	MOFs	12–320	2.7	170	0.3	Two intensities	[189]
	PDMS-eddpo-Ln(bzac)$_3$ (Ln = Eu,Tb)	C	158–248	11	203	5.0×10^{-3}	Two intensities	[240]
	Ln(tfac)$_3$·$2H_2O$ (Ln = Eu, Tb)	C	293–343	7.1	293	9.0×10^{-2}	Two intensities	[131]
	$Sr(HCOO)_2:Eu^{2+}/Eu^{3+}$	MOFs	9–293	3.8	293	–	Two intensities	[188]
	Ln-DPA (Ln = Eu, Tb)	C	293–333	1.5	293	0.3	Two intensities	[180]
	$Eu(bzac)_3(H_2O)_2$	C	188–303	1.4	293	–	Lifetime	[171]
	Ln(btfa)$_3$(H_2O)$_2$ (Ln = Eu, Tb)	C	295–315	5.8	296	0.5	Two intensities	[128]
	$NaGdF_4:Yb^{3+}/Ho^{3+}/Ce^{3+}$@$NaYF_4$ Yb^{3+}/Tm^{3+}	CS	298–393	4.4	298	–	Two intensities	[210]
	$Eu(CPDK_{3.5})_3$phen	C	298–348	2.2	298	–	Lifetime	[241]
	Ln-cpda (Ln = Eu, Tb)	MOFs	40–300	16	300	–	Two intensities	[187]
	$NaYF_4:Yb^{3+}/Er^{3+}$@SiO_2	UCNPs	300–900	1.0	300	1.0	Two intensities	[196]
	$Gd_2O_3:Yb^{3+}/Er^3$	UCNPs	301–350	1.5	301	0.3	Two intensities	[154]
	Eu^{3+}/RhB-based polymer	C	300–310	3.6	302	1.0	Two intensities	[123]
	Eu^{3+}/RhB-based polymer	C	300–310	3.8	302	0.8	Two intensities	[124]
	$NaGd(MoO_4)_2:Tb^{3+}/Pr^{3+}$	P	303–483	5.3	303	–	Two intensities	[242]
	$Eu(bzac)_3(H_2O)_2$	C	188–303	5.3	303	0.1	Single intensity	[171]
	$NaGdF_4:Yb^{3+}/Er^{3+}$@$SiO_2:Eu^{3+}$	CS	293–323	2.7	303	6.0×10^{-2}	Two intensities	[195]
		CS	293–323	2.5	303	0.5	Single intensity	[195]
	$Eu(tta)_3$(pyphen)	C	283–323	1.7	323	–	Lifetime	[243]
	$NaY_2F_5O:Yb^{3+}/Er^3$	UCNPs	298–333	2.8	333	–	Lifetime	[56]
	$MPr(PO_3)_4$ (M = Na, Li, K)	P	298–363	0.60	363	0.8	Two intensities	[172]
	PrP_5O_{14}	P	298–363	0.60	363	0.9	Lifetime	[172]
	$Y_2O_3:Tb^{3+}/Tm^{3+}$	NPs	323–1123	0.33	750	–	Two intensities	[212]
BW-I	$YAlO_3:Nd^{3+}$	NPs	290–610	1.8	293	0.9	Bandwidth	[167]
	$KLuWO_4:Tm^{3+}/Ho^{3+}$	UCNPs	300–333	2.8	300	0.1	Two intensities	[132]
	$NaGdF_4:Er^{3+}/Ho^{3+}/Yb^{3+}$	CS	293–323	1.1	323	–	Two intensities	[217]
BW-II	$YVO_4:Nd^{3+}$	NPs	123–398	0.54	123	–	Two intensities	[198]
	$NaGdF_4$: Nd^{3+}	NPs	298–323	2.5	303	–	Two intensities	[54]
	$NaYF_4:Yb^{3+}/Nd^{3+}$	NPs	125–450	2.5	365	–	Two intensities	[218]
	$YAlO_3:Nd^{3+}$	NPs	290–370	3.3	370	0.3	Two intensities	[167]
BW-II/III	$LaF_3:Er^{3+}/Yb^{3+}$@ $LaF_3:Yb^{3+}/Tm^{3+}$ (*)	UCNPs	293–323	5.0	293	0.3	Two intensities	[125]

A molecule or chemical group able to interact with Li-ion is used as a probe and modifies the optical response of the probe (luminescence/absorbance). An example is presented on **Figure 10** [44].

[44] S. Liu, et al., J. of Colloid and Interface Science (2017) 493.

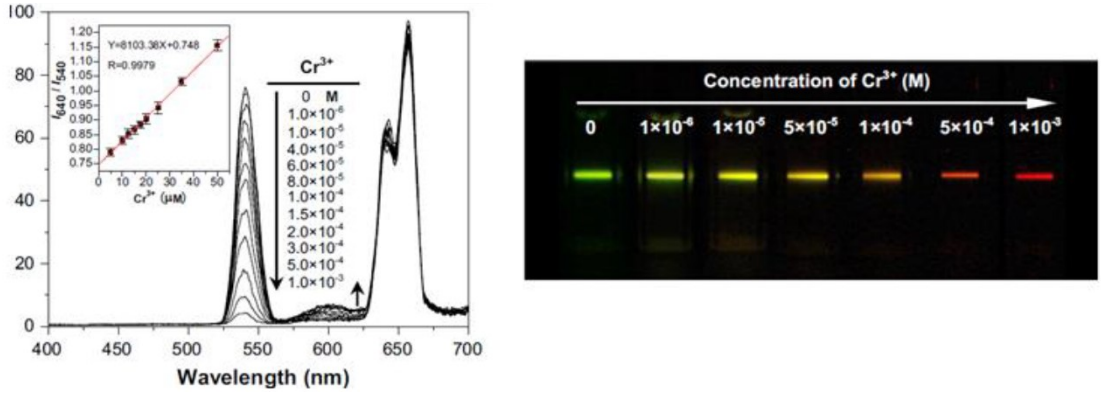

Figure 10. Examples of photoluminescence detection of ions into liquid medium (in the case of Cr^{3+}).

This type of molecule was so far used in solution (water or biologic medium[45]) or incorporated into a porous polymer and used in sensors developed for biological applications[46]. However, this type of probe cannot work in the electrochemical environment of a battery: it is therefore necessary to adapt the chemical nature of the molecule and also the sensor's matrix.

To illustrate the limitation and drawback of the current technology developed for Li-ion concentration measurement, an example of Li-ion sensor is detailed by A. N. Maliya[47]. In this study, the development of a smart device is describe based on molecule, which are able to detect and quantify Li-ion chemistry. This molecule was incorporated into a polymer coating and micro device based on resistive measurement to measure the concentration of Li^+. The principle used here is the modification of resistance of the coating by Li-ion interaction with molecules. This type of sensor has shown good selectivity (lithium compared to potassium and sodium ions), time response and sensitivity. However, the size of the sensor is too big for use inside a cell (3x3 mm for the sensing area, but in the order of the by cm including the Printed Circuit Board). Finally, the sensor was developed and tested into aqueous solution with good results.

The development of luminescent Li ion probe is very active in the field of health and biology. See a recent review from W. Chen et al. gives an overview of the luminescent probe for PH and alkali metal ions[48]. All of this probe is developed for aqueous media and dedicated to the biological application[42]. The challenge in this project is to adapt this probe to the chemistry of the battery electrolyte.

In conclusion, to use this type of probe into the battery environment, it is necessary to adapt the chemistry of the probe to be compatible with the electrolyte medium. The size, thermal and electrochemical stability are also a major constraint for this type of probe.

2.3 Photo-Acoustic gas sensor (PA)

The temperature of LIBs can rise due to the migration of Li-ions and the electrochemical reaction, and in general this temperature rise will not adversely affect the performance and the safety of LIBs at normal conditions. However, if there is an abuse that induces additional heat in the battery, the internal electrochemical side reaction can be intensified, generating a large amount of heat with flammable gases and may lead to a thermal runaway event. This kind of common abuse is schematically presented in **Figure 11**.

[45] F. Berghmans, et al., Proceedings of EWSHM (2014) hal-01021256.

[46] (a) X. Wang, et al., Chem. Soc. Rev. (2013) 42. (b) J. P. Golden, et al., IEEE Transactions on Biomedical Engineering (1994) 41. (c) G. P. Anderson, et al., IEEE Transactions on Biomedical Engineering (1994) 41.

[47] A. N. Mallya, et al., Materials Research Express (2019) 6.

[48] W. Chen et al. Coordination Chemistry Reviews 427 (2021) 213584

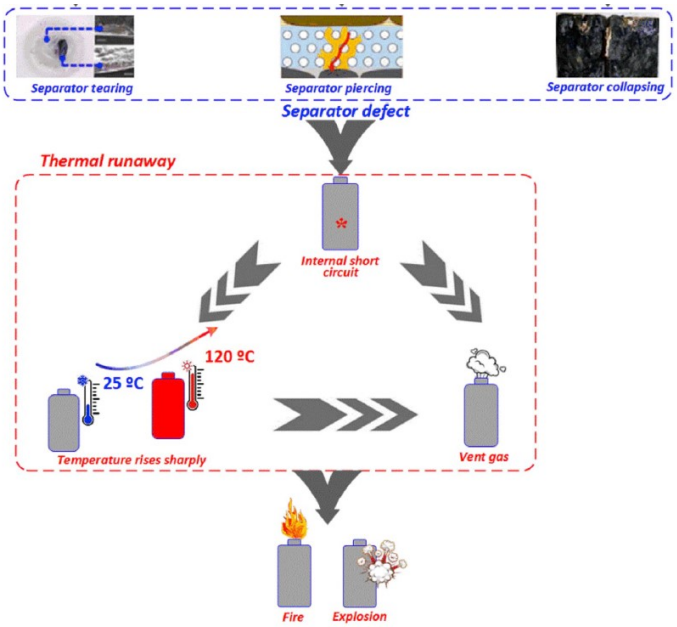

Figure 11. Schematic diagram of the thermal runaway mechanism of LIBs under various sources of abuse (Adapted by Z.Liao et al.)[49]

When LIBs are subject to abuse from various sources, cascade reactions occur resulting in thermal runaway processes that mainly incorporate the following steps: the SEI decomposes, the anode collapses, the intercalated lithium reacts with the electrolyte, the separator melts, the cathode's active substances and the electrolyte lithium salt decompose, the electrolyte solvent oxidizes, the intercalated lithium reacts with the binder, the ceramic coating of separator collapses, and the internal short-circuit occurs. During these periods, not only the temperature of a Li-ion battery changes abruptly, but also a fair amount of gas is also released. During SEI decomposition, the temperature of Li-ion batteries can reach up to 80 to 120 °C, and the metastable substance in the SEI will decompose and produce CO_2, O_2, and some flammable hydrocarbon[50].

In other contexts (e.g. for the determination of ambient air quality) CO_2 detectors are widely used[51]. However, these are usually macroscopic detectors, like diffusion pipes or handheld devices, which in addition do not allow a continuous measurement. Recently, IFAG partner has used microelectronic and mechanical technologies to develop a compact engineering prototype of a sensor based on the photoacoustic principle to control the CO_2 concentration inside of vehicles.

Figure 12 schematics the main basic components using PA effect.

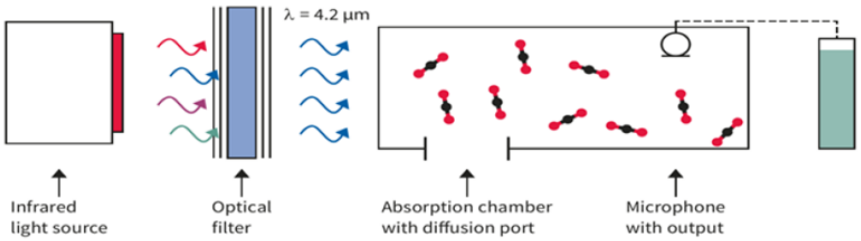

Figure 12. Basic components of a gas sensor based on the photo-acoustic effect.

[49] Z. Liao, et al., J. Power Sources (2019) 436.

[50] Z. Liao, et al., J. Power Sources (2019) 436.

[51] M. Eberl, et al., GMM-Fb. (2019) 93.

Several different embodiments of this sensor have already been manufactured and tested by IFAG, but their principle is always very similar: A thermal emitter generates radiation in the infrared, with blackbody characteristics. The emitted light is periodically chopped and then passed through an optical filter which only allows the dominant excitation wavelength of the gas under analysis to pass (e.g. λ = 4.2 µm for CO_2). The filtered light enters an absorption chamber with a diffusion port, which is filled with gas from the atmosphere of interest. As CO_2 selectively absorbs at 4.2 µm, the energy in the vibration states of the CO_2 molecules in the absorption chamber is increased. Collisions between the molecules transfer this energy into an increase of the temperature (and respectively pressure). The periodic modulation of the radiation source results in a continuous pressure wave in the chamber, which is the equivalent of a sound wave. A very sensitive microphone in the CO_2-filled chamber, manufactured for instance with Micro-Electro-Mechanical System (MEMS) technologies at relatively low cost, can measure this sound.

When the concentration of CO_2 in the absorption chamber increases, more energy is absorbed. This results in an amplification of the sound wave and a correspondingly stronger signal received by the microphone, allowing a correlation between the CO_2 concentration and the output of the microphone. Other gases absorb at different wavelengths, e.g. methane at 3.3 µm. A change in intensity at that wavelength because of the presence of methane does not change the intensity at 4.2 µm, so there is no risk of cross sensitivity.

The dimensions of IFAG's prototype sensor system are currently 14 mm x 12.5 mm x 7 mm, which is significantly smaller than existing CO_2 sensors in the market, but still too large to be directly integrated into a LIB cell. Therefore, further work on integration approaches is required, which also need to consider the compatibility of the sensor with the electrochemical environment within the cell.

Direct and indirect photoacoustic systems both employ the photoacoustic effect for gas detection but differ fundamentally in their setups and working principles. When designing a gas-sensing system, one therefore must be aware of the distinct factors that influence their respective performances in terms of selectivity, sensitivity, stability, robustness, and potential for miniaturization. For setups of indirect photoacoustic spectroscopy, the selectivity of the system is introduced via the gas filling of the hermetically sealed photoacoustic cell. An acoustic signal may only be generated when the emission spectrum of the light source and the absorption spectrum coincide. The gas filling hence acts as a near-ideal spectral filter and the gas to be detected can be chosen according to the requirements of the measurement task. On the other hand, selectivity in direct photoacoustic setups is entirely dependent on the spectral function of the light source, since an acoustic signal will be generated whenever a molecule absorbs radiation. For this reason, thermal emitters are usually combined with spectral filters in order to improve selectivity. Most setups use lasers as light sources because it enables the construction of specific gas detection systems[52].

The use of the photoacoustic effect in gas sensing has a longstanding history, but current research and development efforts show that the potential of the technique is far from fully exploited. In particular, the use of MEMS technology in gas sensing systems will probably lead to further improvements in terms of the long-term stability, miniaturization, integration, and selectivity[53].

2.4 Reference electrode (RE) sensor

In the electrochemical field, the 3-electrodes cell configuration is very often used to measure the potential and the impedance of the working electrode (WE) and the counter electrode (CE) with respect to the reference electrode (RE) which is the third electrode integrated into the cell. Ideally, the suitable electrode reference must present the following typical characteristics: non-polarizability, reliability and reproducibility[54]. Such sensor has been implemented in LIB cells in the aim to have a better understanding of the aging mechanisms and aging

[52] S. Palzer. SENSORS (2020) 20, 2745.

[53] S. Palzer. SENSORS (2020) 20, 2745.

[54] F. La Mantia, C.D. Wessells, H.D. Deshazer, Y. Cui, Electrochem. Commun. 31 (2013) 141–144.

assessment and a lot of studies reports results data obtained on 3-electrodes cells. It is noteworthy that the implementation of a RE sensor has been more recently strongly used to evaluate in operando the potential polarization on the negative electrode that is influenced by the mechanical aging effects. Such degradation favors lithium plating phenomena in charge[55].

But the authors pointed out the difficulty to obtain reliable and reproducible signal[56]. Indeed, the reference electrode arrangement could affect the impedance measurement[57]. Therefore, it has been recognized that the reference electrode has to be positioned inside the electrochemical cell and symmetrically compared with the positive and negative electrodes in order to avoid potential shifts or artifacts on the impedance spectra impedance distortion. Moreover, the design of the RE has also a strong impact towards the signal reliability. Finally, the stability in time is also a criterion to consider that could be particularly selective to compare the potential electrochemical couples.

Experimentally, the integration of a RE sensor inside LIB cells is complex because of the winding or stacking cell conception and by the fact that the cell should be sealed to operate properly.

At a laboratory level, most studies reported in the literature characterize 3-electrodes LIB cells in coffee bags with a design allowing exiting a third tab easily through the heat-sealed laminated aluminum foil[58] (**Figure 13**) But such instrumentation can be realized when the cell is already assembled or on commercial cells[59]. As shown in **Figure 14** that is performed in situ once the cell is assembled and charged[60].

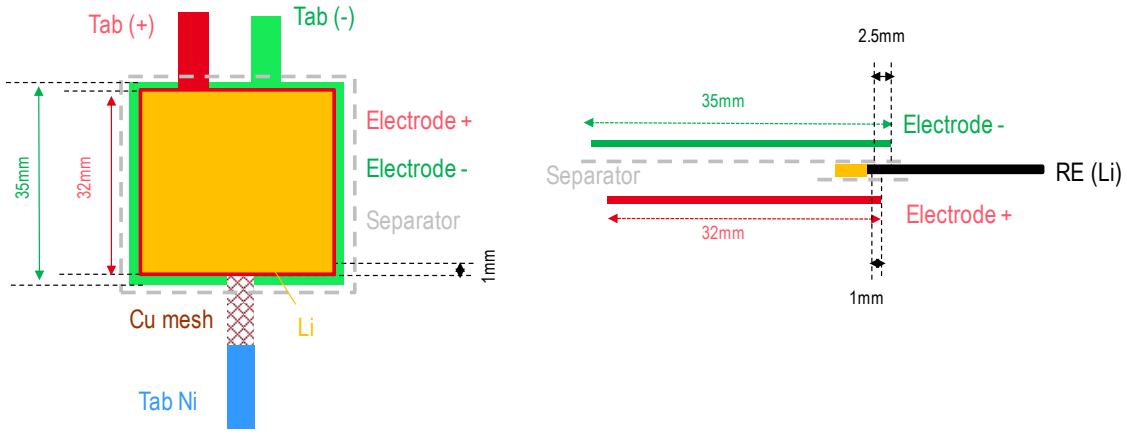

Figure 13. CEA laboratory cell assembly with integrated RE sensor (Li type).

[55] (a) E. McTurk, et al., J. Power Sources (2018) 379. (b) T. Amietszajew, et al., Electrochimica Acta (2018) 263.

[56] Rinaldo Raccichini, Marco Amores and Gareth Hinds, Batteries 2019, 5, 12.

[57] M. Ender, A. Weber, E. Ivers-Tiffée, J. Electrochem. Soc. 159 (2012) A128.

[58] (a) M.-S. Wu, et al., J. Electrochem. Soc. (2005) 152. (b) M. Dollé, et al., J. Electrochem. Soc. (2001) 14.8. (c) I. Jiménez Gordon, et al., Solid State Ionics (2013) 237. (d) X. Hu, et al., J. of Power Sources, 2012 (198).

[59] B. Pilipili Matadi, et al., J. Electrochem. Society (2017) 164.

[60] I. Jiménez Gordon, et al., Solid State Ionics (2013) 237.

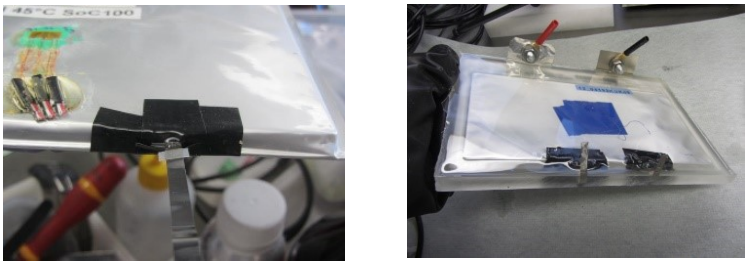

Figure 14. Cell assembly with integrated RE sensors.

Several electrochemical couples for the RE can be used including metallic lithium (Li^+/Li)[61], insertion materials $Li(1-x)FePO_4$/ $LiFePO_4$ (LFP), $Li_4Ti_5O_{12}$/ $Li(4+x)Ti_5O_{12}$ (LTO)[62] , alloy (Li_xAl/Al)[63] or noble metals (**Table 2**). They are identified as possible reference material because their insertion/disinsertion curves show a voltage plateau on a large state of lithiation range. Some of them have to be partially delithiated (LFP) or lithiated (LTO, alloy) to place the insertion potential of the material on the plateau.

The stability in time appears more and more crucial in the perspective to develop innovative smart cells. Today, the challenge is clearly oriented towards the improvement of the potential stability in time of the RE via more effective material like alloys. It could also be planned to re-lithiate the active material of the RE regularly to avoid any shift of the potential according to the same protocol effected initially. Difficulties to overcome to be able to use the RE as in situ diagnostic tool in LIB is discussed in reference [64].

Table 2. *Electrochemical couples used as reference electrode.*

Electrochemical couples	Potential *vs.* Li^+/Li	Observation
Li+/Li	0V	Is usable immediately
$Li_{(1-x)}FePO_4/LiFePO_4$	3.424V	LFP Has to be "activated" before use. It consists to perform in situ a delithiation process to place the insertion potential of the material on the plateau.
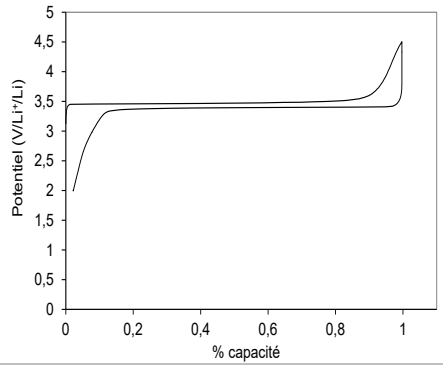		

[61] J. Zhou, et al., J. Electrochem. Soc. (2004) 151.

[62] F. La Mantia, et al., Electrochemistry Communications (2013) 31.

[63] I.G. Kiseleva, et al., Soviet Electrochemistry (1982) 18.

[64] R. Raccichini, et al., Batteries (2019), 5(1), 12.

Li_xAL/Al [65]	0.360V	Aluminum as to be "activated": lithiation process to place the insertion potential of the material on the plateau The state of lithiation must be limited to avoid a too huge volume expansion that could reduce the mechanical integrity of the material.
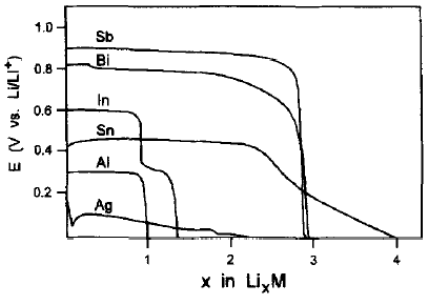		
Noble metals (Pt, Au)		Is usable immediately

The challenges in the practical implementation of such a RE for Li-ion technology to be overcome can be summarized as two basic challenges: first, the conductivity of the cell interior, especially of the electrolyte is rather limited, so the electrolyte at different spots in the cell can be at a different potential. To minimize this effect, electrodes with a relatively large area are employed instead of a simple wire or grid. However, the relatively large conductivity of the electrode in turn modifies the potential distribution in the cell relative to standard cells. Second, any metal or metal-like structure in the cell becomes part of the electrochemical system of the cell. This leads over time to the formation of interface layers on the RE, which, in the best case, only results in a linear (= independent of the potential) change of the electrode electrical resistance requesting sophisticated voltage measurement techniques with infinitesimally small current flow. In the worst case, these interface layers become battery elements on their own, and the voltages measured with the RE do not indicate the status of the LIB cell under surveillance anymore but are only a function of the RE itself.

3. **Conclusions**

This deliverable summarizes a detailed review of the last advances reported in the literature and identify the most interesting solutions, taking them on-board for the developments of four different physical sensors and their integration in the LIB cells. In this way, and considering the provide knowledge by the recent state-of-the-art, the following four physical sensors will be developed/adapted to be integrated in LIB cells:

- Optical Fiber/Fiber Bragg Grating; to monitor temperature, heat flows, and strain/pressure inside the LIB cells.
- Reference electrode; for estimating/measuring "absolute" potential, impedance and polarization.
- Optical Fiber/Luminescence; to monitor temperature, heat flows and Li-ion concentrations.
- Photo-acoustic sensor; to monitor/detect gas concentration (CO_2)

[65] J.O. Besenhard, J. Yang, W. Xinter, J. Power Sources, 68 (1997) 87-90